# Scalar Control of Single-Phase Induction Motor Using PV Fed Modified Seven Level H-Bridge Inverter with Improved Sinusoidal PWM Technique

Ashok Suryawanshi<sup>1\*</sup>, Nilkanth Chopade<sup>1</sup>, Hrishikesh Mehta<sup>2</sup>

<sup>1</sup>Department of Electronics and Telecommunication, Pimpri Chinchwad College of Engineering, Savitribai Phule Pune University, Pune, India

<sup>2</sup>Research and Development, Aethertec Innovative Solutions, Vidnyan Nagar, Bavdhan, Pune, India \*Corresponding author: ashok.suryawanshi@pccoepune.org

Abstract: This paper proposes an improved modulation technique to control a modified H-Bridge solar photovoltaic (PV) fed seven-level inverter to drive a single-phase 230V, 1/2 HP capacitor start-run induction motor (IM). An improved H-bridge 7-level inverter topology is achieved by reducing the number of switches required to produce seven distinct voltage levels. The speed of the IM is controlled using the concept of scalar control. The pulse width modulation (PWM) signals applied to the switches of the 7-level inverter are generated using a combination of three identical sine wave signals. This combination acts as reference signals, which have an offset equal to the amplitude of the triangular carrier signal. The proposed method is implemented in MATLAB / Simulink® environment, and its result demonstrates that the seven-level inverter can successfully suppress harmonics by more than 50% as compared to the three and five-level inverter without the use of an external LC filter. Moreover, the voltage stress across switches is reduced by 35% even though a smaller number of switches are used in the proposed method.

**Keywords:** Pulse width modulated (PWM), seven-level inverter, total harmonic distortion (THD), scalar control, induction motor (IM), Solar PV, MPPT Boost

### I. Introduction:

The endeavor to employ alternative fuels encourages a quick rise in carbon exhaust emissions prices, resulting in long-term CO<sub>2</sub> concentration in the atmosphere (Kazmierkowski et al. 2011). Among the different cleaner energy, sunlight is exquisite with zero greenhouse gas pollutants, and the photovoltaic (PV) technology makes power conversion simple (Rahim, Chaniago, and Selvaraj 2011). It has become a popular source of power for both residential and commercial users (Mishra 2015). This includes solar electric vehicles (EVs), automobile charging points, a significant number of water hydraulic pumps, and freestanding systems for places where the grid connection is unavailable (Metry et al. 2016).

Solar PV (SPV) panels are used to generate photovoltaic electricity, and the output of each panel is supplied into a DC source through a rectifier. The DC-AC converter and the load receive power from a DC link (Saleh and Sumner 2018). SPV production is not continuous, as it varies depending on irradiance and temperature (Hannan et al. 2018). As a result, it is critical to harvest maximum generated power from the PV unit, which is known as maximum power point tracking (MPPT) (Bana et al. 2019), for effective functioning of PV panels even under diverse climatic fluctuations in an annual computation. The DC-DC converter plays an integral role in managing peak energy only when MPPT

is present in a unit since it operates on controlled switching frequency adjustment (Himour and Iffouzar 2020)

Multilevel inverter (MLI) has been chosen in the current scenario focused on the important prerequisite of a DC-AC power converter in a PV, instead of on traditional inverters such as VSI, because it is effective in capable of extracting the supply reliability with substantially less error (Lashab et al. 2021). In comparison to traditional inverters including the flying-capacitor type (FCT) (Hareesh and Jayanand 2021), modern multilayer inverter designs employ a fewer number of circuit components. MLIs are power converters that perform numerous conversions in voltage-based levels and provide improved energy quality, reduced switching inefficiencies, improved system reliability, and high-voltage capabilities. They have been around for approximately twenty years. As a result, among these advantages, multilevel converters have become increasingly popular in recent years (Poorfakhraei, Narimani, and Emadi 2021). The benefits are especially noticeable in standard-size motors used in commercial processes. The diode-clamped, FCT and cascaded H-bridge (CHB) designs have been among the most famous multilevel inverter techniques developed throughout the years (Khasim et al. 2021). In the diode-clamped inverter, many capacitors in series divide the DC bus voltage separating capacitor voltages, generating the voltage levels.

Capacitors are impossible to maintain, notably since there are many of them. Moreover, because of impartial balancing problems, a three-phase iteration with this system is hard to formulate. In comparison to traditional converters such as the FCT (Salem et al. 2021), CHB (Roy and Sadhu 2021), and neutral point clamped type (NPC)(Sameeullah and Chandel 2016). Present multilevel inverter schemes employ a fewer number of components in the system. The quantity of circuit components grows in lockstep with the number of different levels in MLI, increasing complexity and overall cost (Almakhles et al. 2020). Capacitor voltage equalization is a difficult issue between FC-MLI and NPC-MLI since both are confined to five levels and therefore unable to cascade.

It thus reduces the voltage level to 1/2 with those of the inputs, resulting in a higher duty cycle but higher losses (Bhaskar et al. 2020). Varieties of studies have been conducted to reduce the elements of MLI, and numerous designs have been recommended depending on the various layers that face obstacles (Dhanamjayulu et al. 2020),(Mukundan et al. 2020). Isolated and non-isolated MLIs are the two types. A separate DC source is used in isolated inverters, whilst a single source is used in non-isolated inverters (Mondol et al. 2020). In addition, standalone inverters are classified as symmetrical or asymmetrical. The symmetrical design of MLI with lookup tables or binary techniques has an identical value for each DC source; however, the alternative option of MLI with lookup tables or binary techniques has varied values for DC sources (Ponnusamy et al. 2020).

Numerous alternative topologies are compatible with either of the arrangements suggested in (Siddique, Mekhilef, et al. 2020). The asymmetrical design is ideal for solar power generation in low to moderate systems, where PV module tuning may be done fast. When choosing between isolated and non-isolated systems for PV penetration, isolated MLI is the best option. The adjustment of voltage for non-isolated MLI like FCT and NPC, on the other hand, is a difficult problem (Siddique, Alamri, et al. 2020). In the domain of high-power medium-voltage power networks, multi-level proposed converter had lately emerged as a must-have option. MLI generates voltages with stepped waveforms at their output using a mix of semiconductor switches and capacitor voltage sources. These inverters outperform typical inverters in several ways, especially in high-power situations (Khan et al. 2020).

A few of the benefits of such MLI was that it yielded almost sinusoidal output voltage waveforms, therefore optimizing the DC output. Consequently, the harmonic content is kept to a minimum. Switching losses are decreased as well (Dhara and Somasekhar 2020). Additionally, the filters needed to regulate the output voltage is low, small, and affordable hardware, leading to a setup that is simpler, lightweight, but less costly. A control approach is required for a PV-fed inverter to produce a steady DC voltage. In a solar standalone PV system, a conventional PI controller is used to choose an appropriate duty cycle for the DC-DC converter considering contrast in the converter result against a benchmark (Shuvo et al. 2019).

The MPPT approach does not allow direct regulation of the DC-DC converter; therefore, alternative approaches have been suggested to address this problem for freestanding photovoltaic energy. Numerous sophisticated approaches, including artificial intelligence (AI), practical swarm optimization (PSO), fuzzy and genetic algorithms (F&GA), have recently demonstrated smart control over data sets to modulate voltages (Vijeh et al. 2019). The decision of an MPPT methodology for the desired purpose is a difficult undertaking since each method does have its own set of advantages and disadvantages (Siddique et al. 2019). Due to various inherent ease of installation, MPPT methods such as hill climbing (HC), perturbance, and observance (P&O) are commonly employed. Existing techniques such as fuzzy, P&O, and INC techniques fail to extract global MPP point (GMPPP) under temporary shade situations (Sahoo and Bhattacharya 2018).

MLI with DCT connection using MPPT has already been developed in several literary works, wherein output regulation may be performed by load capacity (Hota, Jain, and Agarwal 2018) either under stable solar irradiation (Vahedi, Sharifzadeh, and Al-Haddad 2018). MPPT adjusts the output of the solar PV to run at its full capacity, which is determined by temperature, loading, and irradiance. Considering the impact of climate and depending on weather, either solar irradiance level or temperature fluctuate throughout the day. As a result, it's critical to keep track of all these variables to get the most out of MPPP (Ho and Chun 2018). The capability to use DC power on the designated H-bridge cells distinguishes the CHB from other MLIs, leading to energy transformation split across much higher voltages for lower frequency inverters and lower voltages with higher frequency inverters.

Its approach for sequencing two-level and MLIs are described in (Babadi et al. 2018). The advantage of this strategy is that it does not need distinct sources for every step. The advantage of cascaded inverters is that they multiply reference voltage, level resulting in extremely low harmonics. Another benefit is that the large-volume inverter can be bought, however, the major low-power conditional inverter requires special manufacture (Blaabjerg, Gao, and Lim 2009). The cascaded design additionally eliminates the need for such a set of multiple DC voltages, which may be inconvenient in grid-connected energy technologies. Another advantage of the dual inverter design is that it may provide resilience, allowing for remedial action in the event of failure (Tete, Gupta, and Joshi 2021). Such architecture, on the other hand, necessitates the use of independent DC voltage sources. In MLI, managing these topologies becomes more complex as the number of stages grows.

In this paper, the modified H-bridge single-phase MLI control design with characteristics including both diode-clamped and CHB inverters are integrated. Furthermore, as compared to traditional inverters with a similar number of levels, this innovative topology has a lower number of switching devices. An improved sine wave PWM approach is used to eliminate harmonic distortion in a modified architecture of MLIs. In the MATLAB Simulink® environment, the inverter scheme is simulated. The simulation results achieved are displayed to demonstrate that the proposed control is

effective. The modelling of PV and boost converter is illustrated in Section II. The working of a modified single-phase 7-level inverter and improved sine wave PWM technique is illustrated in detail in Section III. Section IV consists of MATLAB / Simulink® implementation and a detailed discussion on its outcomes, while Section V ends with a conclusion and the future scope.

### **II. PV and Boost Converter Modelling**

Photovoltaic modeling is an integral part of assessing a solar PV system. PV Panels have a DC-DC boost converter, and a 7-level MLI are all the part of total proposed topology, which is depicted in Fig. 1. The solar PV system may be calculated using three different approaches, which are I-V characteristics, P-V characteristics, and solar irradiance / temperature having partial shading conditions. PV is a combination of the terms 'photo and voltaic': photo symbolizes photonic energy and voltaic represents electrical energy (Poorfakhraei, Narimani, and Emadi 2021). Implying that the energy is converted from solar-based photons to electricity. A solar PV array is made up of several sorts of modules, each of which contains solar cells. P-N semiconductor diodes are included in this (Khasim et al. 2021). The planned PV tends to change its output when temperature and environmental circumstances change.

As a result, the elements to consider while modeling a solar PV system are listed below:

# a. Solar PV Equivalent circuit

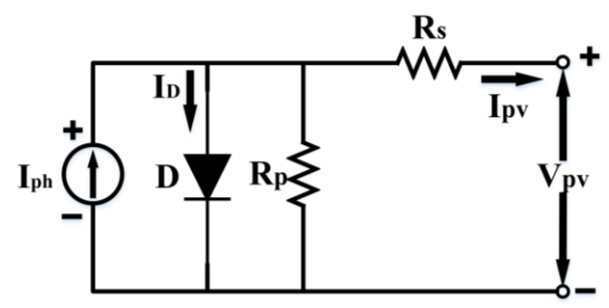


Fig. 1. Solar PV equivalent circuit (Khasim et al. 2021)

Internal resistances  $R_s$  and  $R_p$  are connected in series and parallel, respectively in parallel to the diode in the solar cell, forming an analogous circuit as illustrated in Fig. 1.  $V_{PV}$  = output voltage and  $I_{PV}$  = output current is denoted for a solar cell. These are obtained from Eq. (1) which shows the series/parallel connections of many PVs,

$$I_{PV} = \left\{ I_{ph} - I_0 \times \left[ \exp\left(\frac{q \times (V_{PV} + R_{se} \times I_{PV})}{N_{se} \times AKT}\right) - 1 \right] - \frac{(V_{PV} + R_{se} \times I_{PV})}{N_{par} \times R_{par}} \right\}$$
(1)

Where,  $N_{se}$  = PV cells in series and  $N_{par}$  = PV cells in parallel;  $R_{se}$  = resistance in series;  $R_{par}$  = resistance in parallel; A = ideality factor, K is Boltzmann's constant =  $(1.3806 \times 10^{-23} J/K)$ ; and T = gradient temperature. The  $I_P$  = generated current dependent on irradiance and gradient temperature as shown in Eq. (2) as

$$I_P = \left[I_{SCC-ST} + K_i(T - T_{STM})\right] - \left(\frac{G}{G_{STM}}\right) \tag{2}$$

Where,  $I_{scc-ST}$  is a short-circuited current (SSC) at appropriate test cases at STM;  $K_i$  = short-circuit current coefficient; G (W/m<sup>2</sup>) = irradiance on the cell surface; G<sub>STM</sub> (1000 W/m<sup>2</sup>) = irradiance at STM; and the cell gradient temperature =  $T_{STM}$ .

$$I_{D} = \left\{ \frac{I_{SCC-ST} + K_{i}(T - T_{STM})}{\exp[\left(V_{OCV-ST} + K_{OCV}(T - T_{STC})/AV_{SC\_th}\right)]} \right\}$$
(3)

Where,  $V_{OCV-ST}$  = at the proper testing case of open-circuited voltage,  $K_{OCV}$  = open-circuit (OC) voltage coefficient,  $V_{SC\ th}$  is solar cell thermal voltage,

$$P_{PV} = V_{PV} \times N_{SH} \left[ I_{Ph} - I_{O} exp \left( \frac{q V_{PV}}{N_{SE} AKT} \right) - \left( \frac{V_{PV}}{N_{SE}} \right) \right]$$
 (4)

## b. Boost Converter Equations

A DC-DC boost converter connects with PV to the proposed inverter circuit. The boost converter is made up of a high-frequency inductor (L), capacitors ( $C_1$ ,  $C_2$ ), and switches ( $S_1$ ,  $S_2$ ). Based upon power switches, the boost converter offers three operating modes. The following relationship may be used to compute a converter's output voltage.

$$V_0 = \frac{D}{1 - D} \times V_{in}$$

Where,  $V_0$  = converter output voltage, D = percentage duty cycle and  $V_{in}$  = input DC voltage. The boost converter's critical inductor value is made from,

$$L = \frac{V_{in}}{f_s \Delta I_L}$$

Where,  $f_s$  = switching frequency,  $I_0$  = Output current,  $\Delta I_L$  = inductor current = 0.3 $I_0$  and  $V_{in}$  = input voltage.

The critical value of the capacitor is obtained from,

$$C = \frac{I_0}{(f_s \times \Delta V_0)D}$$

Where,  $\Delta V_0$  = voltage ripple which should be 5% of the total output voltage.

### III. Modified Single-Phase 7-Level Inverter:

### A. Working of Inverter Power Circuit:

A block diagram that represents major blocks of the proposed scheme for open-loop control is shown in Fig. 2 scalar control; PWM generator, 7-level voltage inverter, and single-phase IM are the major blocks in the diagram. The supply frequency is given to the scalar control profile block to generate reference voltage for generating PWM. Accordingly, the PWM block set will generate the PWM pulses required to obtain seven-level output from the inverter.

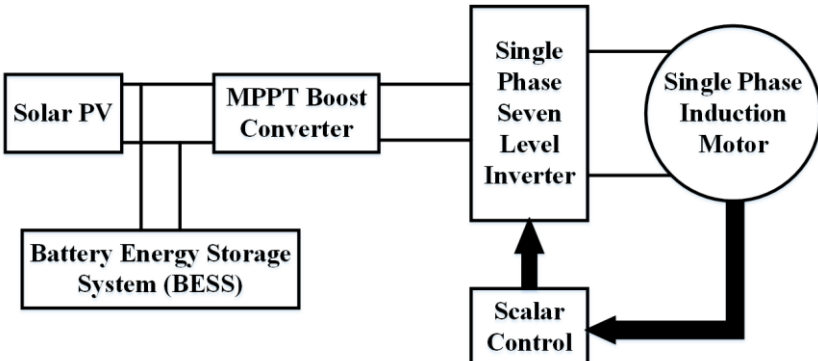


Fig. 2. The proposed open loop scalar control-based scheme control of a single-phase IM using a modified H-bridge 7-level inverter is depicted in a block diagram.

The scalar control is named for the fact that it concentrates on the steady-state dynamic parameters. At the abase speed, the induction motor draws the rated current and produces the rated torque. The magnetic field created by the stator is exactly proportional to the torque provided by the motor. As a result, the voltage provided to the stator is proportional to the flux multiplied by the stator's rotational velocity. As a result, the stator's flux is proportional to the applied voltage and frequency of the supply. The frequency may be altered to vary the motor's speed. Flux and hence torque may be maintained throughout a wide speed range by changing the voltage and frequency in the same proportion.

Stator Voltage 
$$(V_{stator}) \propto \left[ \text{Stator Flux} \left( \varphi_{flux} \right) \right] \times \left[ \text{Angular Velocity} \left( \omega \right) \right]$$

$$V_{stator} \propto \left( \varphi_{flux} \times 2 \times \pi \times freq. \right)$$

$$\varphi_{flux} \propto \frac{V_{stator}}{\text{freq.}}$$

Now, to keep the flux constant, the scalar control ratio must be constant for various speeds. As the speed of the motor is increased, the stator voltages must be increased to keep the scalar control ratio constant. The suggested single-phase 7-level inverter (SP-7LI) is built using a 5-level inverter described in [7] – [11]. As illustrated in Fig. 3, it is made up of a 1-phase traditional H-bridge, 2-bidirectional switches, and a capacitive voltage-based divider circuit comprising  $C_1$ ,  $C_2$ , and  $C_3$ , respectively. The modified H-bridge type architecture provides significant advantages over alternative topologies for inverters with similar levels, such as fewer power electronic-based power switches/diodes, and capacitors. An R or R-L load receives the inverter's output power. With correct switching, the inverter may generate 7-output voltage levels from DC ( $V_{de}$ ). The functioning of suggested inverter type may suitably be divided into seven-switching states, as shown in Fig. 3. Moreover, Fig. 4 {(a), (d), and (g)} show the operational states of a traditional inverter in order, whereas Fig. 4{(b), (c), (e), and (f)} illustrates ancillary conducting states as per proposed inverter that synthesizes  $1^{st}$  and  $2/3^{rd}$  states of the DC-bus voltages.

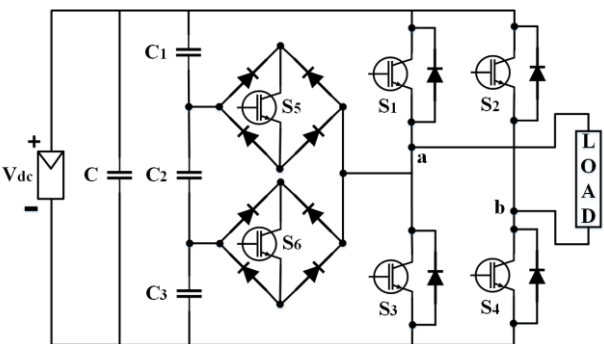


Fig. 3. Proposed single-phase 7 level inverter with modified H-bridge topology

Following are the 7 output voltage levels as follows.

- 1) Output Voltage ( $+V_{dc}$ ): Switch  $S_1$  and  $S_4$  are switched ON, with the positive terminal connected to ( $+V_{dc}$ ) and the negative terminal is connected to the ground. The rest of the switches are OFF and a voltage of  $+V_{dc}$  is applied to the load side terminal, as shown in Fig. 4(a).
- 2)  $2/3^{rd}$  Positive Output (+2V<sub>dc</sub>/3): Switch S<sub>5</sub> connects the positive terminal inclined towards the ground, whereas Switch S<sub>4</sub> connects the negative terminal to the surface. The remaining switches are switched OFF, and a voltage of  $2V_{dc}/3$  is applied to the load terminals. The present active routes are depicted in Fig. 4(b).

- 3)  $1/3^{rd}$  Positive Output ( $V_{dc}/3$ ): Switch  $S_6$  connects the positive terminal to the ground, while Switch  $S_4$  connects the negative port to the ground. Rest of the switches are switched-OFF and load terminals are supplied with  $V_{dc}/3$  voltage. The active routes at this time are shown in Fig. 4(c).
- 4) Zero Output: Switches  $(S_3, S_4)$  are turned-on while remaining switches are switched-OFF. Contact "ab" is clipped, and the voltage supplied to the output load = 0. Active routes are described in Fig.4 (d).
- 5)  $1/3^{rd}$  Negative Output (-V<sub>dc</sub>/3): The connection between the positive-terminal is turned ON at V<sub>dc</sub> by S<sub>5</sub>, whereas the negative terminal is linked at V<sub>dc</sub> by S<sub>2</sub>. The remaining switches are switched-OFF, and a voltage of V<sub>dc</sub>/3 is applied towards the load. The present active routes are depicted in Fig. 4(e).
- **6)**  $2/3^{rd}$  Negative Port Output (- $2V_{dc}/3$ ): Two-way switch  $S_6$  connects the positive port of the battery to the ground, whereas the  $S_2$  switch connects the negative terminal towards the ground. The remaining switches are switched OFF, and the load terminals are supplied with a voltage of  $2V_{dc}/3$ . The current active routes are depicted in Fig. 4(f).
- 7) Maximum Output Negative ( $-V_{dc}$ ): Switches  $S_2$  and  $S_3$  are turned ON, the negative terminal is connected to  $V_{dc}$ , and the positive terminal is connected to the ground. The remaining switches are switched OFF, and a  $-V_{dc}$  voltage is applied to the load-end terminals. The present active routes are depicted in Fig. 4(g).

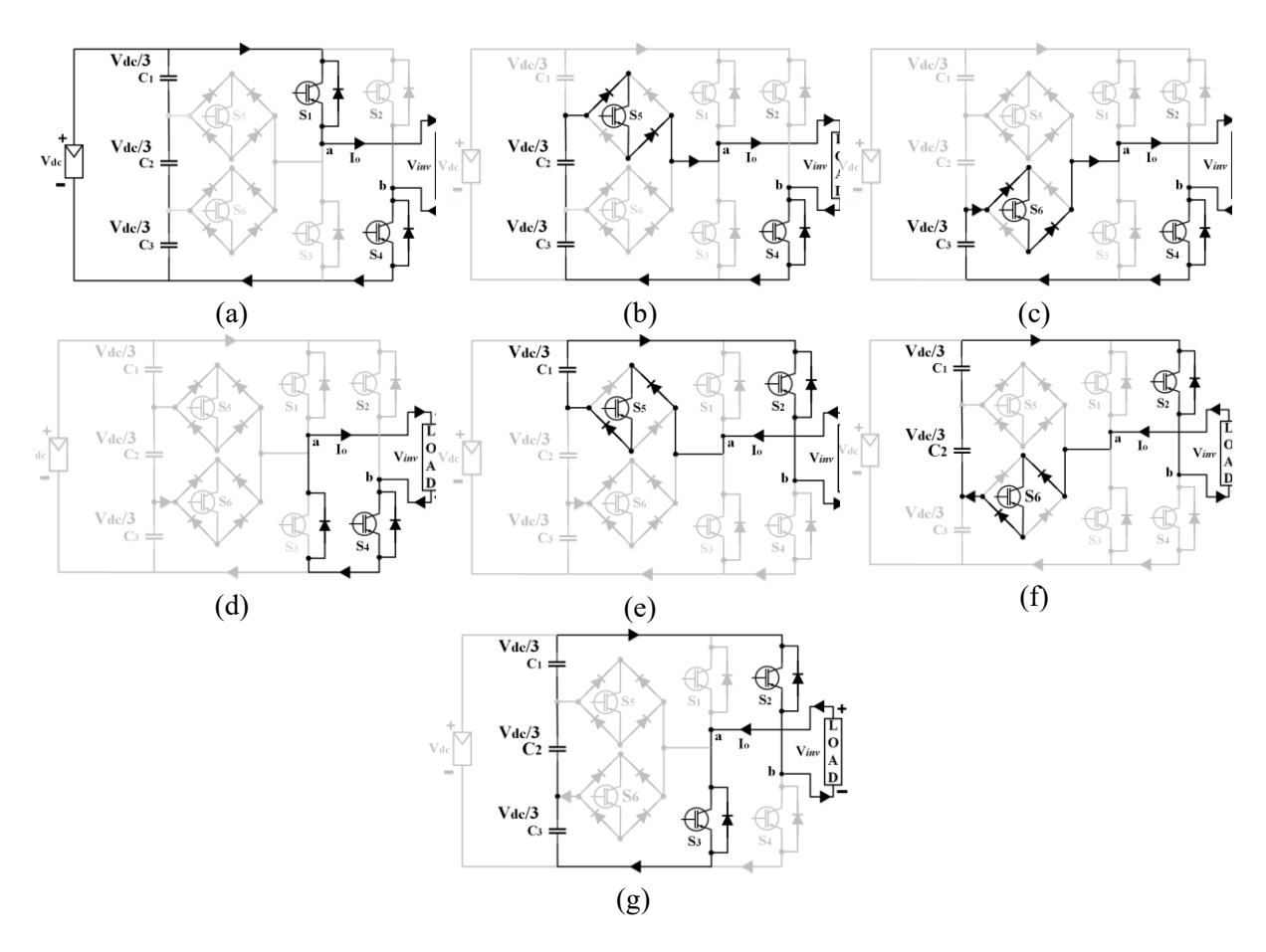


Fig. 4. Classification for output voltage V<sub>dc</sub> when the switching combination is necessary for V<sub>ab</sub>

(a) 
$$V_{ab} = V_{dc}$$
, (b)  $V_{ab} = 2V_{dc}/3$ , (c)  $V_{ab} = V_{dc}/3$ , (d)  $V_{ab} = 0$ , (e)  $V_{ab} = (-2V_{dc}/3)$ , (f)  $V_{ab} = -V_{dc}/3$ , and (g)  $V_{ab} = (-V_{dc})$ 

Table 1. ON/OFF Conditional Output Terminal Voltages of Power Electronic Switches

V <sub>0</sub>	S <sub>1</sub>	S <sub>2</sub>	$S_3$	S <sub>4</sub>	<b>S</b> <sub>5</sub>	S <sub>6</sub>
+V <sub>dc</sub>	ON	OFF	OFF	ON	OFF	OFF
(+2V <sub>dc</sub> /3)	OFF	OFF	OFF	ON	ON	OFF
$(+V_{dc}/3)$	OFF	OFF	OFF	ON	OFF	ON
0	OFF	OFF	ON	ON	OFF	OFF
0*	ON	ON	OFF	OFF	OFF	OFF
$(-V_{dc}/3)$	OFF	ON	OFF	OFF	ON	OFF
$(-2V_{dc}/3)$	OFF	ON	OFF	OFF	OFF	ON
-V <sub>dc</sub>	OFF	ON	ON	OFF	OFF	OFF

The 7-output based voltage levels are described in Table 1. The PWM based signal is produced from a unique PWM-modulation approach. A carrier signal was compared to three distinct signals, viz.,  $V_{carrier} = (V_{ref1}, V_{ref2}, \text{ and } V_{ref3})$ . The distinct reference signals comprising similar type of the frequency and amplitude as per carrier-based signal with an in-phase offset is proportional to the carrier signal's amplitude. The carrier signal was compared to each of the reference signals. The  $V_{ref1}$  would be differentiating from  $V_{carrier}$ . The resultant switching pattern is shown in Fig. 4. Moreover, switches  $(S_1, S_3, S_5, S_6)$  operate at the carrier-based signal frequency, whereas  $(S_2, S_4)$  are intended to operate at the carrier frequency.

### B. Improved Modulation Technique

The suggested inverter functioned in 6-modes for 1-cycle of the main fundamental based frequency. For one cycle, Fig. 5 illustrates the PU (per-unit) voltage output signal ( $V_{output}$ ). Following are the descriptions of the six modes:

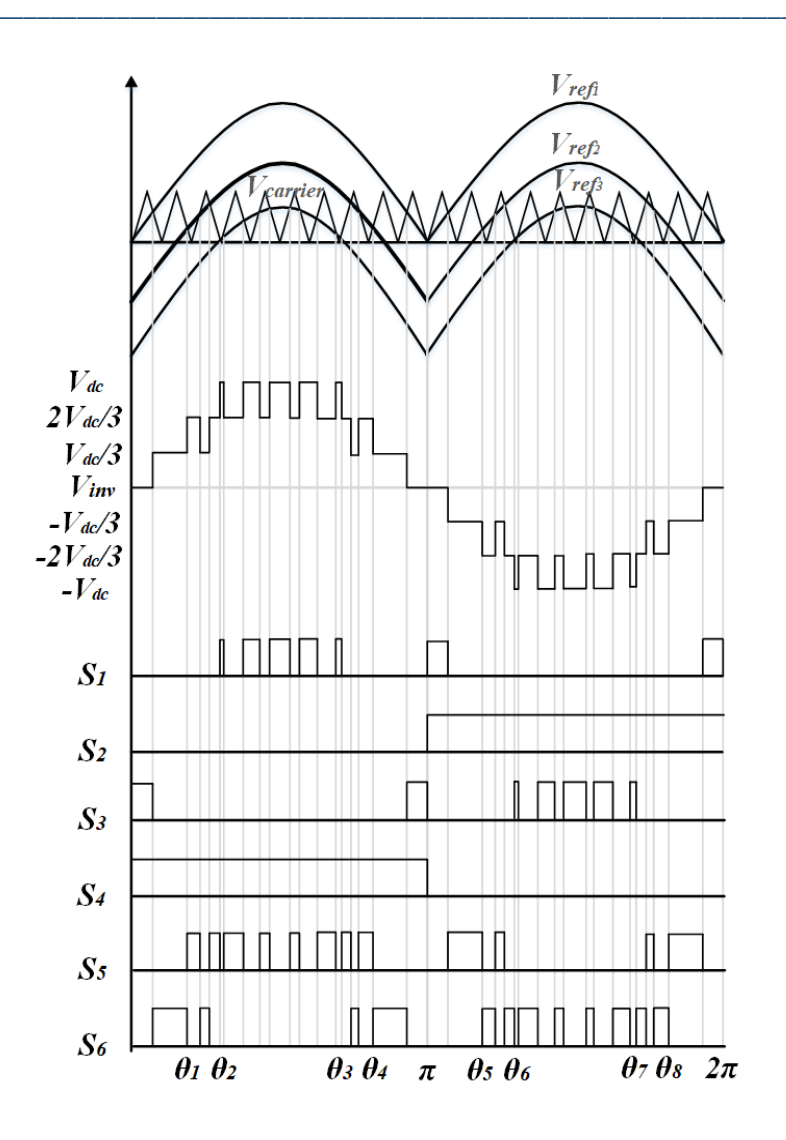


**Fig. 5.** The single-phase 7 level inverter switching pattern.

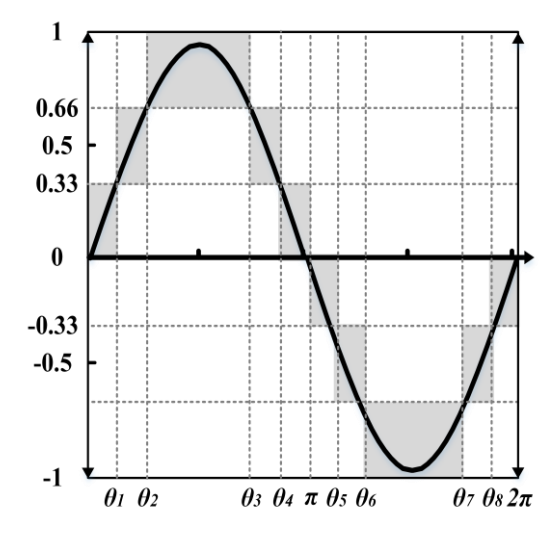


Fig. 6. Illustration of Switching angles and seven-level output voltage (Vab)

\_\_\_\_\_

The suggested inverter works in 6-modes for 1-cycle of the main frequency. For one-cycle, the PU output-voltage signal is shown in Fig. 6. The following are the descriptions of the six modes:

The modes tend to depend up on the modulation-based index  $(M_a)$ . Consequently, with main single reference and carrier signal the modulation is defined as,

$$M_a = \frac{A_{main}}{A_{carrier}}$$

For one main signal and two carrier-based signals the  $M_a$  becomes,

$$M_{a} = \frac{A_{main}}{2 \times A_{carrier}}$$

Similarly, for proposed improved 7-level PWM, the MLI utilizes three carrier-based signals the  $M_a$  becomes

$$M_a = \frac{A_{main}}{3 \times A_{carrier}}$$

Where,  $A_{carrier} = peak$ -to-peak unit of the carrier wave and  $A_{main} = peak$  unit of the reference voltage wave  $V_{ref}$ .

When,  $M_a < 0.33$ , the displacement of per phase-based angle is

$$\theta_1 = \theta_2 = \theta_3 = \theta_4 = \pi \times 0.5$$
  
$$\theta_5 = \theta_6 = \theta_7 = \theta_8 = \pi \times 1.5$$

On the other hand, when  $M_a > 0.33 < 0.66$ , the determination of  $\theta_s$ , s = 1, 2, 4, 5, 6, 8 is

$$\theta_1 = \sin^{-1} \left( \frac{A_{carrier}}{A_{main}} \right)$$

$$\theta_2 = \theta_3 = \pi \times 0.5$$

$$\theta_4 = \pi - \theta_1$$

$$\theta_5 = \pi + \theta_1$$

$$\theta_6 = \theta_7 = \pi \times 1.5$$

$$\theta_8 = 2\pi - \theta_1$$

If,  $M_a < 0.66$ , the determination of  $\theta_s$ , s = 1, 2, 3, 4, 5, 6, 7, 8 is

$$\theta_1 = \sin^{-1}\left(\frac{A_{carrier}}{A_{main}}\right)$$

$$\theta_2 = \sin^{-1}\left(\frac{2 \times A_{carrier}}{A_{main}}\right)$$

$$\theta_3 = \pi - \theta_2$$

$$\theta_4 = \pi - \theta_1$$

$$\theta_5 = \pi + \theta_1$$

$$\theta_6 = \pi + \theta_2$$

$$\theta_7 = 2\pi - \theta_2$$

$$\theta_8 = 2\pi - \theta_1$$

When  $M_a \le 0.33$  to smallest reference wave  $V_{ref3}$  is evaluated to the triangle-based carrier signal. The behaviour of the inverter works similarly to the full-bridge 3-level PWM inverter. When  $M_a > 0.33 < 0.66$ , the  $(V_{ref2}, V_{ref3})$  output is compared with the triangle-based carrier-wave. There are five DC-voltage levels in the output voltage. The  $M_a$  index is kept at 0.66 when 7-levels of  $V_{out}$  is to be created. To create pulses the 3 signals for reference is compared to the triangle-based carrier signal.

# IV. MATLAB Implementation of the Proposed Scheme:

Because of its acute structure for the necessity of few deterministic parameters, the perturbance-and-observance (P&O) method is found in the proposed inverter. It perplexes, the terminal array-based voltage and evaluates the solar PV based output power to the preceding perturbing cycle. The attenuation of perturbance would continue for a certain orientation in the following cycle if the power was gaining; however, the orientation would be changed. It further implies that in every MPPT cycle, the array-based terminal voltage is disrupted; as a result, when the MPP point is achieved, P&O algorithm oscillates around.

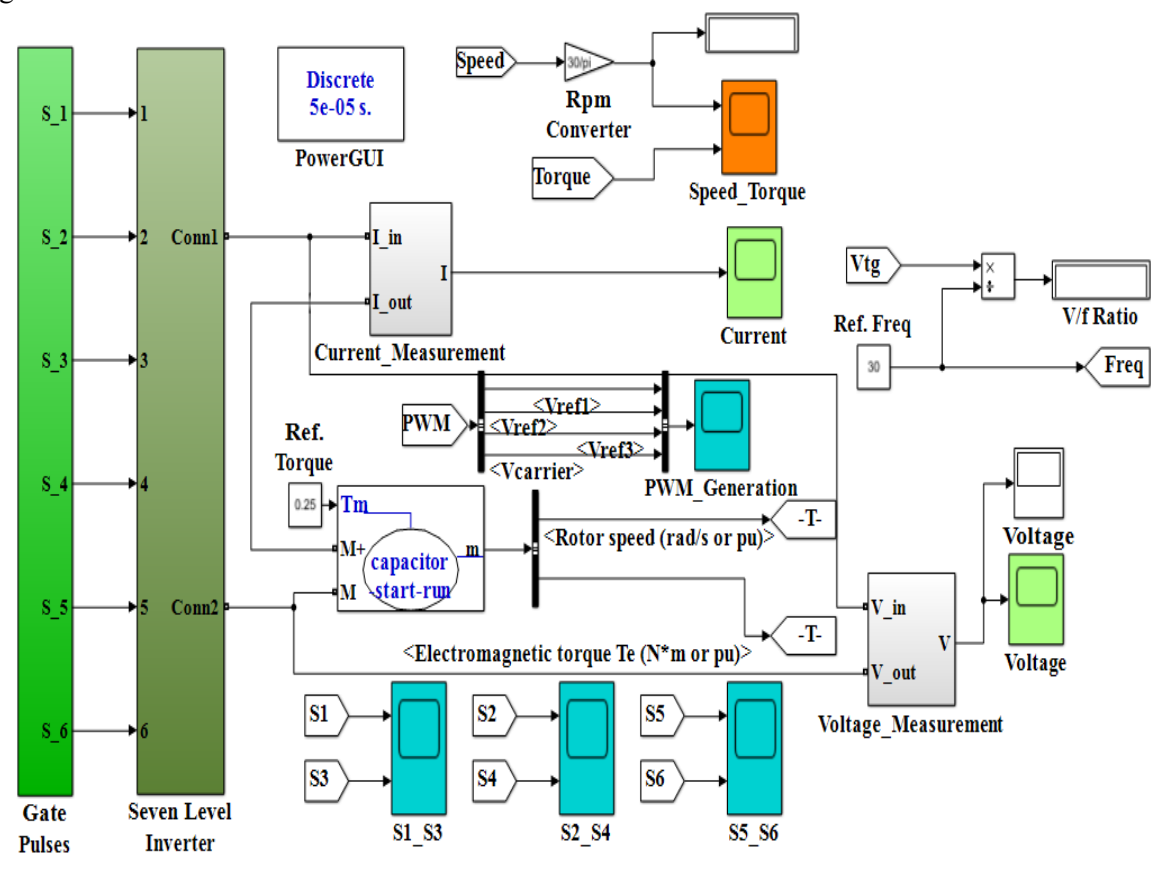


Fig. 7. Single Phase 7-Level Inverter in MATLAB / Simulink® Environment

ISSN: 1001-4055 Vol. 44 No. 4 (2023)

Fig. 8. Cascaded Method of Diode-Clamped Inverter with 7-Levels

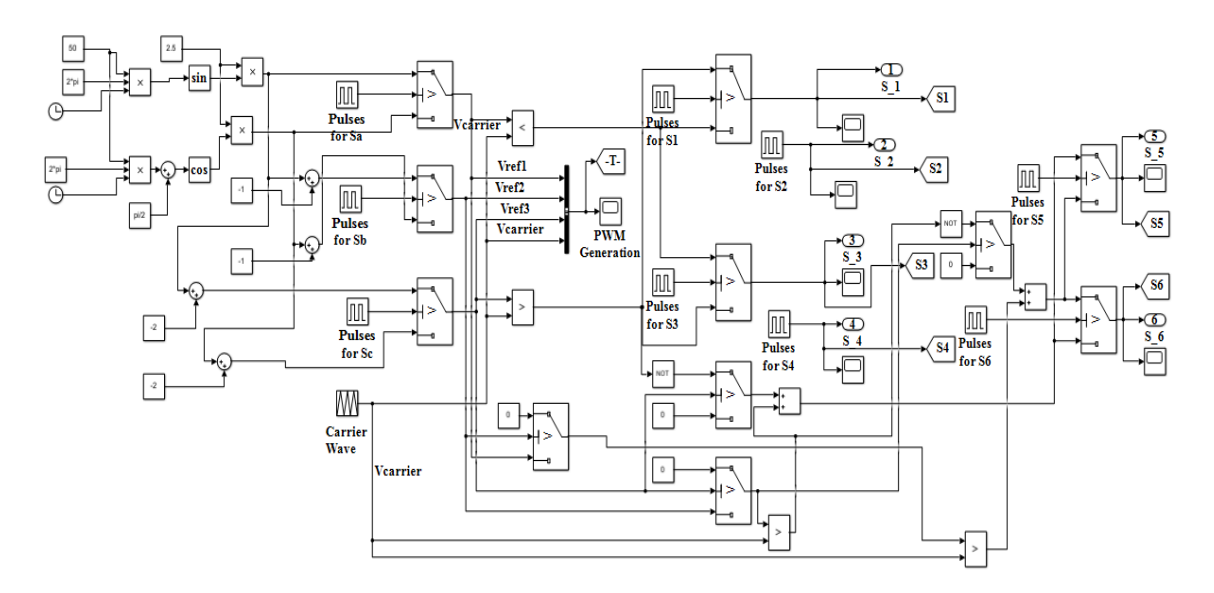


Fig. 9. MATLAB/Simulink® Model of a Seven-Level Single-Phase Inverter

Fig. 7 shows the Simulink model, which includes Inverter Bridge of Cascaded type, gate pulses-based electronic switching, loading arrangements, current-based measurement, and voltage-based measurement systems. The scope in the Simulink® also shows all of the essential measurements. It has a block diagram-like structure. When obtaining results with a pure load resistance, the used R-L load is replaced with a simply R-load. The subsystem consists of DC supply, IGBT switches with diodes and the DC-linked capacitor arrangement is depicted in Fig. 8. Each of the subsystems is thoroughly detailed. The essential steps for creating the seven-level output voltage are generated using three series capacitors of 1mF apiece and one input capacitor of 20mF in tandem. To restrict the current inrush during capacitor charging, a 220V DC supply is provided combined with one series resistance. Fig. 9 shows the evolution of gate pulses for driving these IGBT switches. Three reference waves are created with 180° phase shift using logical switching in which the sine wave utilizes a 3-sine wave function generates a positive sine type wave even in the negative half-cycle.

As a result, just three positive reference waves are created using a switch configuration, and a 6-sine wave function is employed. Fig. 10 depicts the gate pulse development system's configuration. The biases of these three reference waves are compared to a triangle carrier wave with a frequency of 2 kHz. Fig. 11 depicts these signals.

The switching pattern is also created for each of the 6-IGBTs. Fig. 10, 11, and 12 illustrate the gate patterns for the IGBT switch  $(S_1 - S_3)$  pair,  $(S_2 - S_4)$  pair, and  $(S_5 - S_6)$  pair, correspondingly.

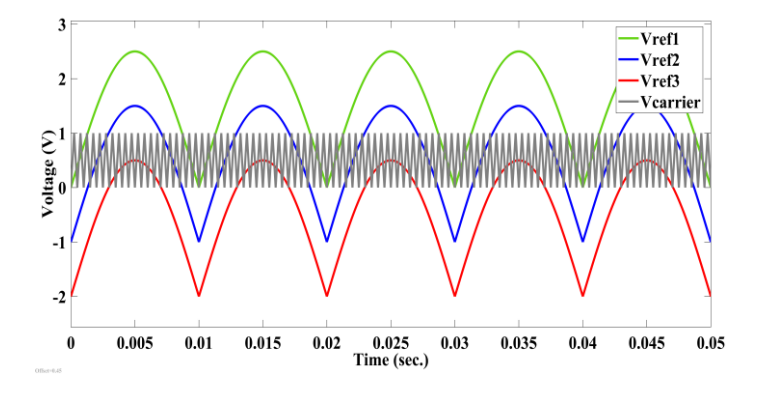
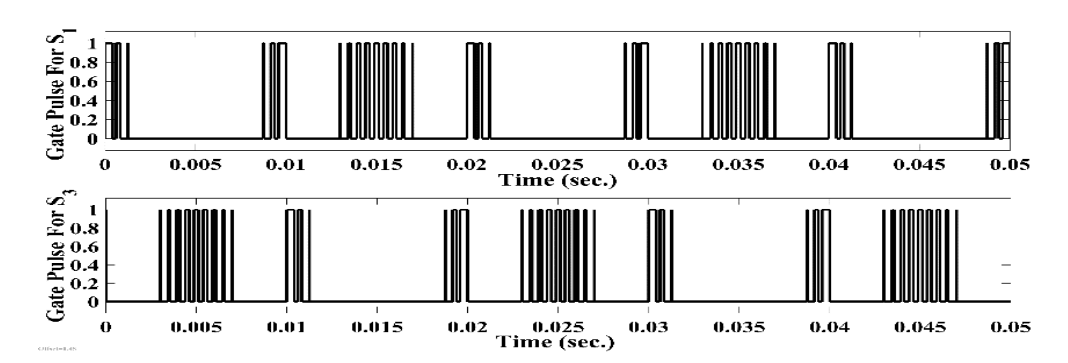


Fig. 10. PWM Generation



**Fig. 11.** Response of Switches  $S_1$  and  $S_3$  based on PWM signals.

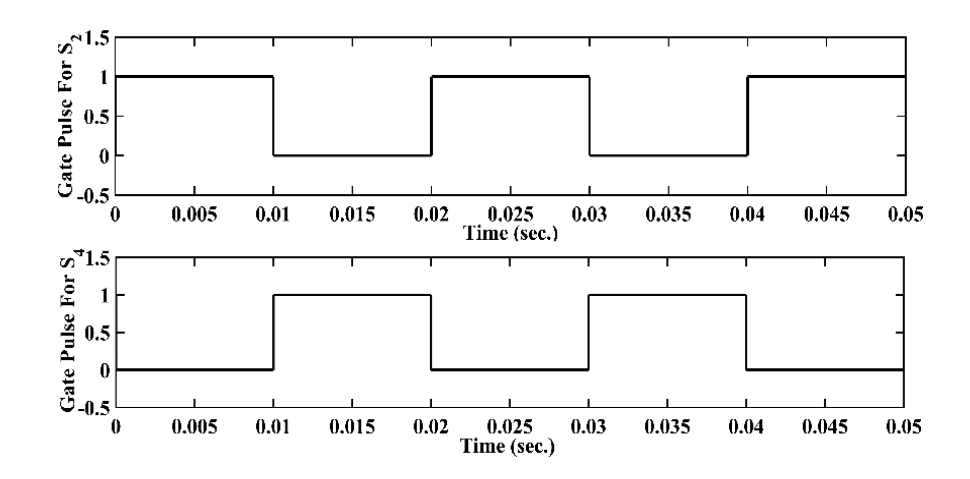


Fig. 12. Response of Switches S<sub>2</sub> and S<sub>4</sub> based on PWM signals.



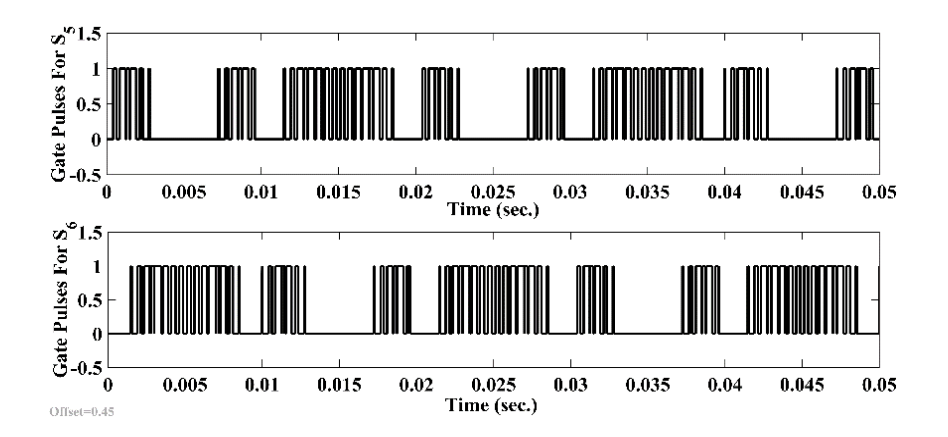


Fig. 13. S<sub>5</sub> and S<sub>6</sub> based PWM signals.

### V. Results and Discussions:

Fig. 14 depicts a seven-level voltage output waveform. The response clearly shows 7-voltage steps levels. The situation is the same for both R and R-L loads. Fig. 14 also shows the instantaneous voltage waveform. Fig. 15 and 16 illustrates current waveforms for R- and RL-loads of  $100 \Omega$  and  $R = 10 \Omega$ ; L = 70mH, respectively. For the RL- load, distortions in the current waveform may be seen.

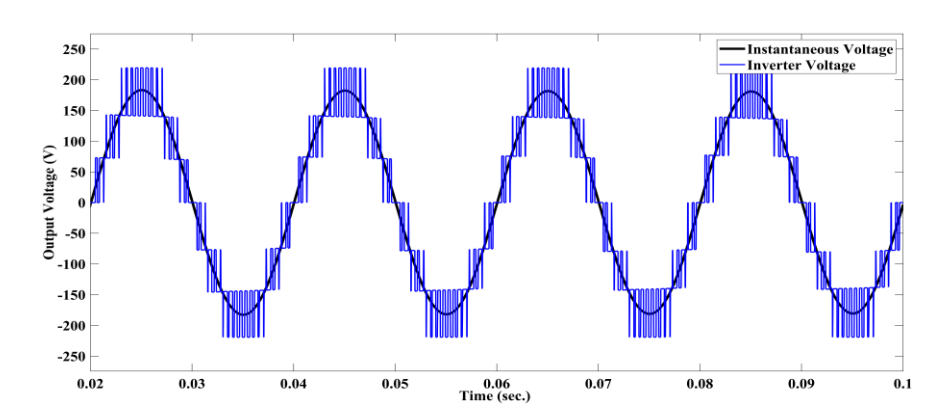


Fig. 14. Output Voltage-Waveform

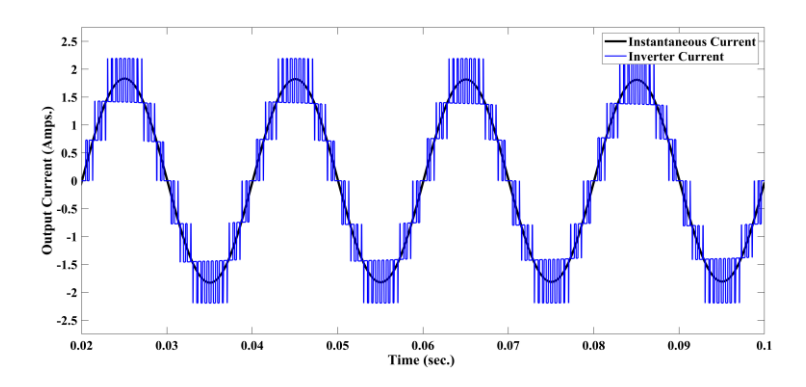


Fig. 15. R-load based Current-Waveform

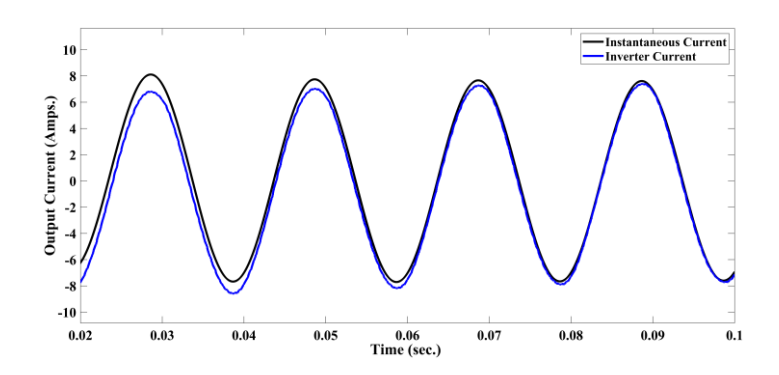


Fig. 16. RL load based Current-Waveform

Figs. 17(a) and 17(b) illustrates FFT analysis utilizing Nyquist frequency to compute THD for the present waveform in the case of R and R-L loads.

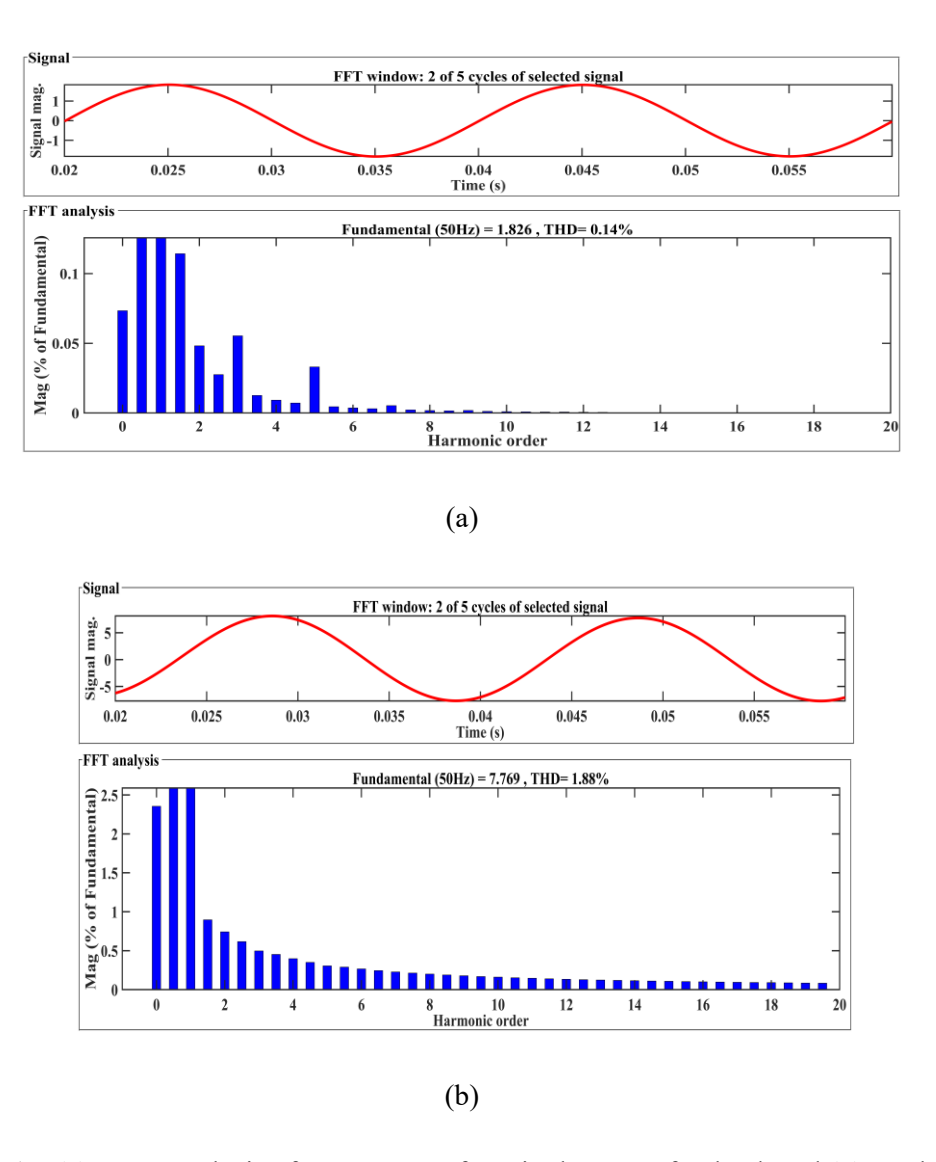


Fig. 17. (a) THD Analysis of current waveform in the case of R-load, and (b) RL-load

Vol. 44 No. 4 (2023)

# A. THD Analysis for 3, 5, And 7 Level Inverter for R- and RL-Load

For expected single-phase 7 levels modified H-bridge inverter, by adjusting the values of modulation index  $(M_a)$ , the output level of the inverter can be controlled.

- **a.**  $M_a \le 0.33$ , the inverter behaves as a typical full-bridge three-level PWM inverter.
- **b.** For  $M_a \sim 0.33$  to 0.66, a five-level output voltage if the inverter is obtained.
- **c.** For  $M_a > 0.66$ , the seven-level output voltage is obtained.

Verification of the effect of THD, the proposed scheme of single-phase inverter is run for various levels of operations under R and RL loads. The value of R- and RL- is  $100~\Omega$  and 0.02H respectively. The graphs representing the percentage THD are shown using the FFT analysis tool in MATLAB / Simulink®.

Case 1: Single-phase 7-level inverter for R-load THD analysis.

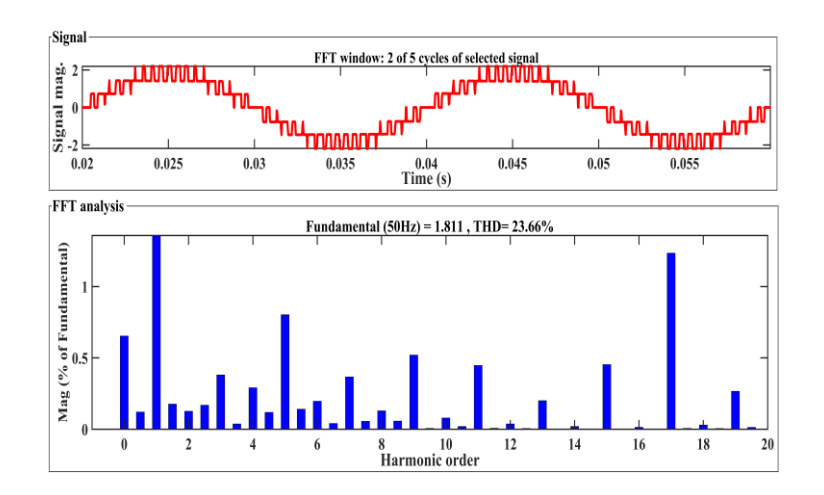
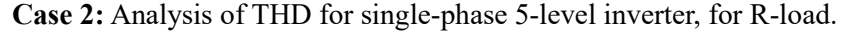


Fig. 18. THD Analysis of Current Waveform with  $M_a = 0.83$ , 7 level, R-load, THD = 23.66%



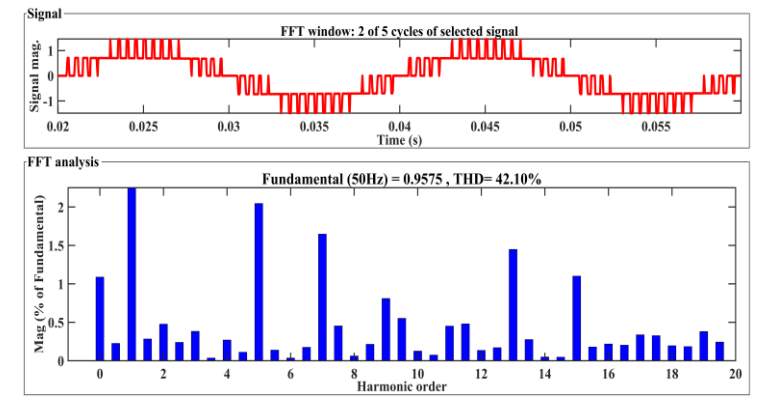


Fig. 19. THD Analysis of Current Waveform with  $M_a = 0.55$ , 5 level, R-load, THD = 42.10% Analysis of THD of Current Waveform in 5-Level Inverter with R-Load

Case 3: Analysis of the THD for single-phase 3-level inverter, for R-load.

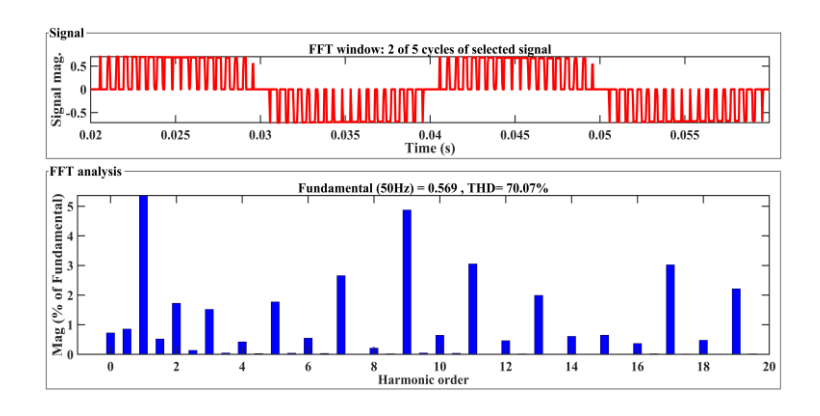


Fig. 20. THD of Current Waveform with  $M_a = 0.33$ , 3 level, R-load, THD = 70.07%

Case 4: Analysis of THD of SP-7MLI single-phase 7-level inverter for RL-load.

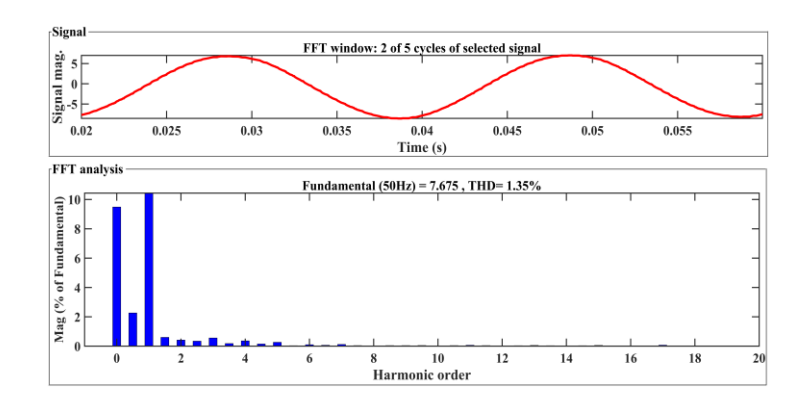


Fig. 21. THD Analysis of Current Waveform with  $M_a = 0.83$ , 7 level, RL-load, THD = 1.35%

Case 5: Analysis of THD of SP-5MLI single-phase for RL load.

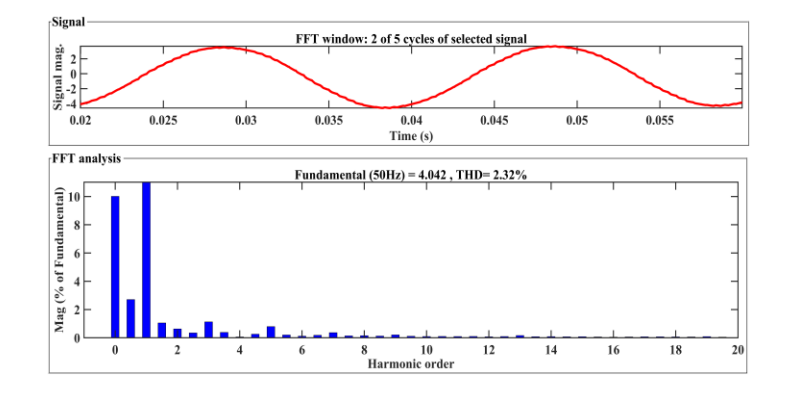


Fig. 22. THD Analysis of Current Waveform with  $M_a = 0.55$ , 5 level, RL-load, THD = 2.32%

**Case 6:** THD analysis of single-phase 3 level inverter for RL load.

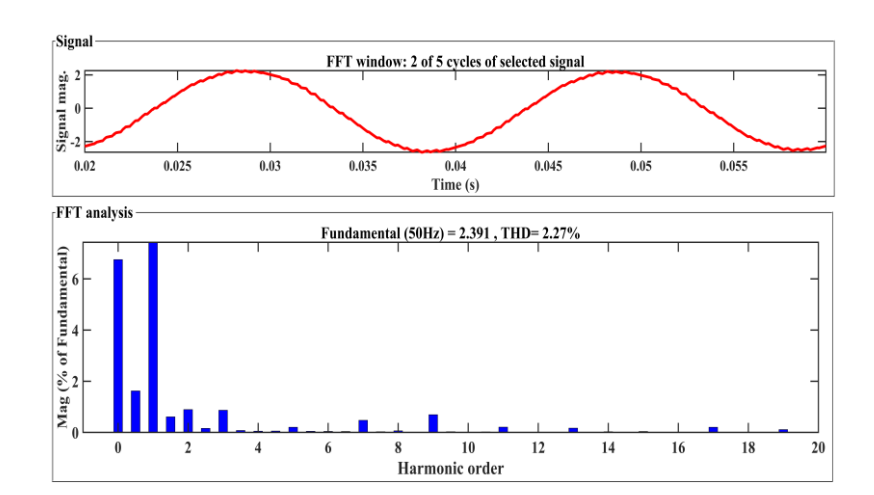


Fig. 23. THD Analysis of Current Waveform with  $M_a = 0.33$ , 3-level, RL-load, THD = 2.27%

Table 2. Comparison of Various Levels of Inverter Output and its THD Analysis for R- and RL-Load

Modulation Index	$M_a = 0.33$	$M_a = 0.55$	$M_a = 0.83$				
$(\mathbf{M_a})$	$(0 < M_a \le 0.33)$	$(0.33 < M_a \le 0.66)$	$(0.66 < M_a \le 1)$				
Type of Inverter	Type of Inverter 3 Level		7 Level				
Type of Load $R = 100 \ \Omega$							
THD%	<b>THD%</b> 70.07 42.10 23.66						
$R = 100 \Omega, L = 0.02 H$							
THD%	2.27	2.32	1.35				

Table 2 represents the output of current waveforms and its THD-based analysis for 3-, 5-, and 7-level output of inverter-based topology considering R- and RL-load. Observations for R and RL load; as the output-based level of inverter is increased, the percentage of THD goes on decreasing. For three-level inverter output, the percentage of THD is more as compared to seven-level inverter output for R and RL load conditions. These THD percentages are significantly lower than those reported in [12] for three-level and five-level inverters with identical inverter architecture. The proposed inverter design has successfully achieved reduced distortion in the current-based waveforms. This will suitably be useful for a single-phase induction motor concerning regulation in speed using the proposed scalar control-based control technique.

<b>Table 3.</b> Operation of Motor for different	Voltages and frequencies
--	--------------------------

$V_{dc}(V)$	Vtg. (V)	Freq. (Hz)	Speed (N)	T (Nm)	V/f	I (A)
398	229.9	50	1474	2	4.48	4.23
372	206	45	1329	2.09	4.57	7.71
342	184	40	1166	2.04	4.61	11.09
315	161	35	938	1.87	4.60	14.77
294	136.5	30	835	1.79	4.59	11.46
276	114	25	710	1.85	4.54	11.79

Table 3 shows the various parameters of the motor for the corresponding change in reference frequency. Here reference torque is kept constant to 2N-m. As the frequency is changed in the step size of 5Hz there is a change in all parameters of the motor which can be seen from the table. It can be noted that as the frequency of the motor decreases, the applied stator voltage is also decreased to keep the scalar ratio is kept constant at a 4.6 value. Table 4 annotates that voltage remains constant as the motor is loaded by incremental steps of 0.5 N-m, but the frequency drops slightly. This change can be observed in the increasing scalar ratio. In addition, developed torque is the same as applied torque.

Table 4. Performance of the Motor for Varying Torque

T (Nm)	Vtg. (V)	Speed (RPM)	Scalar Control	I (A)	T <sub>dev</sub> (Nm)
0.5	230.1	1493	4.62	3.8	0.5
1	230.2	1487	6.64	3.9	0.99
1.5	229.9	1482	4.65	4.2	1.5
2	230.1	1476	4.67	4.3	1.99
2.5	230.1	1468	4.69	4.46	2.49
3	230	1460	4.72	4.8	2.99

The PV panels are selected of 36V, 100W of 4 each. As the motor is considered of 230V, 0.5HP, the type of the MPPT used is P&O. The boost converter converts the voltage from 120V to 350V. Moreover, the motor runs at the full load with output power and efficiency. From Table 5, with a change in the number of MLI levels, the PV power and motor power allow to decrease the percentage THD from 23.71% to 6.74% and at the same time increase the efficiency from 94.83% to 97.24%, respectively.

**Table 5.** Performance of Motor Varying Solar Conditions

Sr.	Inverter	PV Power	Motor Power	Efficiency	Percentage THD
No.	Level	(W)	(W)	(η)	(%)
1.	2-Level	370	350.9	94.83	23.71
2.	3-Level	371.4	355.2	95.63	14.68
3.	5-Level	373.2	357.1	95.68	9.45
4.	7-Level	374	363.70	97.24	6.74

### VI. Conclusion:

The modified H-bridge single-phase 7-level inverter is proposed in this research. The voltage levels were driven with an improved sine wave PWM technique, and the results reveal the 7-level inverter voltage based output levels as  $(V_{dc})$ ,  $(2V_{dc}/3)$ ,  $(V_{dc}/3)$ ,  $(V_{dc}/3)$ ,  $(-V_{dc})$ ,  $(-2V_{dc}/3)$ ,  $(\frac{-V_{dc}}{3})$ . Its design was simulated in MATLAB / Simulink® environment. The R- and RL-load findings as well as the percentage THD are discussed in this study. By altering the  $M_a$  based on its percentage THD these 7-level inverter outputs were compared with three and five-level inverters utilizing the identical inverter arrangement. This inverter was also put to the test using a single-phase IM. The suggested inverter was used to drive 0.5HP IM utilizing a scalar control approach. The results demonstrate that this approach of speed control is effective. It may be concluded that the suggested system is completely implementable in real-world applications and can demonstrate that it improves their power quality.

# **Acknowledgments:**

This work was supported by the Aethertec Innovative Solutions, Baydhan, Pune, India.

### **References:**

- [1] Almakhles, Dhafer J., Jagabar Sathik Mohamed Ali, Sanjeevikumar Padmanaban, Mahajan Sagar Bhaskar, Umashankar Subramaniam, and Rathinasamy Sakthivel. 2020. "An Original Hybrid Multilevel DC-AC Converter Using Single-Double Source Unit for Medium Voltage Applications: Hardware Implementation and Investigation." *IEEE Access* 8: 71291–301. https://doi.org/10.1109/ACCESS.2020.2986932.
- [2] Babadi, Adel Nazemi, Omid Salari, Mohammad Jafar Mojibian, and Mohammad Tavakoli Bina. 2018. "Modified Multilevel Inverters with Reduced Structures Based on PackedU-Cell." IEEE Journal of Emerging and Selected Topics in Power Electronics 6 (2): 874–87.

- https://doi.org/10.1109/JESTPE.2017.2767499.
- [3] Bana, Prabhat Ranjan, Kaibalya Prasad Panda, R. T. Naayagi, Pierluigi Siano, and Gayadhar Panda. 2019. "Recently Developed Reduced Switch Multilevel Inverter for Renewable Energy Integration and Drives Application: Topologies, Comprehensive Analysis and Comparative Evaluation." *IEEE Access* 7: 54888–909. https://doi.org/10.1109/ACCESS.2019.2913447.
- [4] Bhaskar, Mahajan Sagar, Dhafer Almakhles, Sanjeevikumar Padmanaban, Dan M. Ionel, Frede Blaabjerg, Jiangbiao He, and A. Rakesh Kumar. 2020. "Investigation of a Transistor Clamped T-Type Multilevel H-Bridge Inverter with Inverted Double Reference Single Carrier PWM Technique for Renewable Energy Applications." *IEEE Access* 8: 161787–804. https://doi.org/10.1109/ACCESS.2020.3020625.
- [5] Blaabjerg, Frede, Feng Gao, and Sok Wei Lim. 2009. "Operational Analysis and Modulation Control of Three-Level Z-Source Inverters With Enhanced Output Waveform Quality." *IEEE Transactions on Power Electronics* 24 (7): 1767–75. https://doi.org/10.1109/TPEL.2009.2014651.
- [6] Dhanamjayulu, C., Shaik Reddi Khasim, Sanjeevikumar Padmanaban, G. Arunkumar, Jens Bo Holm-Nielsen, and Frede Blaabjerg. 2020. "Design and Implementation of Multilevel Inverters for Fuel Cell Energy Conversion System." *IEEE Access* 8 (Dcm): 183690–707. https://doi.org/10.1109/ACCESS.2020.3029153.
- [7] Dhara, Sumon, and V. T. Somasekhar. 2020. "An Integrated Semi-Double Stage-Based Multilevel Inverter with Voltage Boosting Scheme for Photovoltaic Systems." *IEEE Journal of Emerging and Selected Topics in Power Electronics* 8 (3): 2326–39. https://doi.org/10.1109/JESTPE.2019.2955729.
- [8] Hannan, M. A., Jamal A. Ali, Azah Mohamed, and Aini Hussain. 2018. "Optimization Techniques to Enhance the Performance of Induction Motor Drives: A Review." *Renewable and Sustainable Energy Reviews* 81 (May): 1611–26. https://doi.org/10.1016/j.rser.2017.05.240.
- [9] Hareesh, A., and B. Jayanand. 2021. "Scalar and Vector Controlled Infinite Level Inverter (ILI) Topology Fed Open-Ended Three-Phase Induction Motor." *IEEE Access* 9 (Ili): 98433–59. https://doi.org/10.1109/ACCESS.2021.3096125.

[10] Himour, Kamal, and K. Iffouzar. 2020. "A Random PWM Control Strategy for a Three-Level Inverter Used in a Grid Connected Photovoltaic System." *International Journal of Power Electronics and Drive Systems* 11 (3): 1547–56. https://doi.org/10.11591/ijpeds.v11.i3.pp1547-1556.

- [11] Ho, Anh Vu, and Tae Won Chun. 2018. "Single-Phase Modified Quasi-Z-Source Cascaded Hybrid Five-Level Inverter." *IEEE Transactions on Industrial Electronics* 65 (6): 5125–34. https://doi.org/10.1109/TIE.2017.2779419.
- [12] Hota, Arpan, Sachin Jain, and Vivek Agarwal. 2018. "An Improved Three-Phase Five-Level Inverter Topology with Reduced Number of Switching Power Devices." *IEEE Transactions on Industrial Electronics* 65 (4): 3296–3305. https://doi.org/10.1109/TIE.2017.2758722.
- [13] Kazmierkowski, Marian P., Leopoldo G. Franquelo, Jose Rodriguez, Marcelo A. Perez, and Jose I. Leon. 2011. "High-Performance Motor Drives." *IEEE Industrial Electronics Magazine* 5 (3): 6–26. https://doi.org/10.1109/MIE.2011.942173.
- [14] Khan, Md Noman Habib, Mojtaba Forouzesh, Yam P. Siwakoti, Li Li, and Frede Blaabjerg. 2020. "Switched Capacitor Integrated (2n + 1)-Level Step-Up Single-Phase Inverter." *IEEE Transactions on Power Electronics* 35 (8): 8248–60. https://doi.org/10.1109/TPEL.2019.2963344.
- [15] Khasim, Shaik Reddi, C. Dhanamjayulu, Sanjeevikumar Padmanaban, Jens Bo Holm-Nielsen, and Massimo Mitolo. 2021. "A Novel Asymmetrical 21-Level Inverter for Solar PV Energy System with Reduced Switch Count." IEEE Access 9: 11761–75. https://doi.org/10.1109/ACCESS.2021.3051039.
- [16] Lashab, Abderezak, Dezso Sera, Frederik Hahn, Luis Juarez Camurca, Marco Liserre, and Josep M. Guerrero. 2021. "A Reduced Power Switches Count Multilevel Converter-Based Photovoltaic System with Integrated Energy Storage." *IEEE Transactions on Industrial Electronics* 68 (9): 8231–40. https://doi.org/10.1109/TIE.2020.3009594.
- [17] Metry, Morcos, Sertac Bayhan, Mohammad B. Shadmand, Robert S. Balog, and Haitham Abu Rub. 2016. "Sensorless Current Model Predictive Control for Maximum Power Point Tracking of Single-Phase SubMultilevel Inverter for Photovoltaic Systems." *ECCE* 2016 *IEEE Energy*

Conversion Congress and Exposition, Proceedings. https://doi.org/10.1109/ECCE.2016.7855423.

- [18] Mishra, Ruchi. 2015. "Simulation Model of a Three Phase Multilevel Inverter for a Grid Connected Photovoltaic System." *Intl J Engg Sci Adv Research* 1 (1): 106–12. chrome-extension://efaidnbmnnnibpcajpcglclefindmkaj/viewer.html?pdfurl=https%3A%2F%2Fweb.a rchive.org%2Fweb%2F20180421125806id\_%2Fhttp%3A%2F%2Fwww.ramauniversityjourn al.com%2Fengineering%2Fpdf\_file%2F106-112.pdf&clen=712727&chunk=true.
- [19] Mondol, Md Halim, Mehmet Rida Tür, Shuvra Prokash Biswas, Md Kamal Hosain, Shuvangkar Shuvo, and Eklas Hossain. 2020. "Compact Three Phase Multilevel Inverter for Low and Medium Power Photovoltaic Systems." *IEEE Access* 8: 60824–37. https://doi.org/10.1109/ACCESS.2020.2983131.
- [20] Mukundan, C. M.N., P. Jayaprakash, Umashankar Subramaniam, and Dhafer J. Almakhles. 2020. "Binary Hybrid Multilevel Inverter-Based Grid Integrated Solar Energy Conversion System with Damped Sogi Control." *IEEE Access* 8 (Mli): 37214–28. https://doi.org/10.1109/ACCESS.2020.2974773.
- [21] Ponnusamy, Prem, Pandarinathan Sivaraman, Dhafer J. Almakhles, Sanjeevikumar Padmanaban, Zbigniew Leonowicz, Matheswaran Alagu, and Jagabar Sathik Mohamed Ali. 2020. "A New Multilevel Inverter Topology with Reduced Power Components for Domestic Solar PV Applications." *IEEE Access* 8: 187483–97. https://doi.org/10.1109/ACCESS.2020.3030721.
- [22] Poorfakhraei, Amirreza, Mehdi Narimani, and Ali Emadi. 2021. "A Review of Modulation and Control Techniques for Multilevel Inverters in Traction Applications." *IEEE Access* 9: 24187–204. https://doi.org/10.1109/ACCESS.2021.3056612.
- [23] Rahim, Nasrudin A., Krismadinata Chaniago, and Jeyraj Selvaraj. 2011. "Single-Phase Seven-Level Grid-Connected Inverter for Photovoltaic System." *IEEE Transactions on Industrial Electronics* 58 (6): 2435–43. https://doi.org/10.1109/TIE.2010.2064278.
- [24] Roy, Tapas, and Pradip Kumar Sadhu. 2021. "A Step-Up Multilevel Inverter Topology Using Novel Switched Capacitor Converters with Reduced Components." *IEEE Transactions on*

Industrial Electronics 68 (1): 236–47. https://doi.org/10.1109/TIE.2020.2965458.

- [25] Sahoo, Saroj Kumar, and Tanmoy Bhattacharya. 2018. "Phase-Shifted Carrier-Based Synchronized Sinusoidal PWM Techniques for a Cascaded H-Bridge Multilevel Inverter." *IEEE Transactions on Power Electronics* 33 (1): 513–24. https://doi.org/10.1109/TPEL.2017.2669084.
- [26] Saleh, Kamel, and Mark Sumner. 2018. "Sensorless Control of a Fault Tolerant Multi-Level Inverter PMSM Drives in Case of an Open Circuit Fault." SPEEDAM 2018 - Proceedings: International Symposium on Power Electronics, Electrical Drives, Automation and Motion, 883–88. https://doi.org/10.1109/SPEEDAM.2018.8445360.
- [27] Salem, Ahmed, Huynh Van Khang, Kjell G. Robbersmyr, Margarita Norambuena, and Jose Rodriguez. 2021. "Voltage Source Multilevel Inverters with Reduced Device Count: Topological Review and Novel Comparative Factors." *IEEE Transactions on Power Electronics* 36 (3): 2720–47. https://doi.org/10.1109/TPEL.2020.3011908.
- [28] Sameeullah, Malik, and Sunita Chandel. 2016. "Design and Analysis of Solar Electric Rickshaw: A Green Transport Model." 2016 International Conference on Energy Efficient Technologies for Sustainability, ICEETS 2016, 206–11. https://doi.org/10.1109/ICEETS.2016.7582927.
- [29] Shuvo, Shuvangkar, Eklas Hossain, Tanveerul Islam, Abir Akib, Sanjeevikumar Padmanaban, and Md Ziaur Rahman Khan. 2019. "Design and Hardware Implementation Considerations of Modified Multilevel Cascaded H-Bridge Inverter for Photovoltaic System." *IEEE Access* 7: 16504–24. https://doi.org/10.1109/ACCESS.2019.2894757.
- [30] Siddique, Marif Daula, Basem Alamri, Farhan A. Salem, Mohamed Orabi, Saad Mekhilef, Noraisyah Mohamed Shah, N. Sandeep, et al. 2020. "A Single DC Source Nine-Level Switched-Capacitor Boost Inverter Topology with Reduced Switch Count." *IEEE Access* 8: 5840–51. https://doi.org/10.1109/ACCESS.2019.2962706.
- [31] Siddique, Marif Daula, Saad Mekhilef, Muhyaddin Rawa, Addy Wahyudie, Bekkhan Chokaev, and Islam Salamov. 2020. "Extended Multilevel Inverter Topology with Reduced Switch Count and Voltage Stress." *IEEE Access* 8: 201835–46. https://doi.org/10.1109/ACCESS.2020.3026616.

[32] Siddique, Marif Daula, Saad Mekhilef, Noraisyah Mohamed Shah, Adil Sarwar, Atif Iqbal, Mohammad Tayyab, and Mohsin Karim Ansari. 2019. "Low Switching Frequency Based Asymmetrical Multilevel Inverter Topology with Reduced Switch Count." *IEEE Access* 7: 86374–83. https://doi.org/10.1109/ACCESS.2019.2925277.

- [33] Tete, Pranjali R., Mahendra M. Gupta, and Sandeep S. Joshi. 2021. "Developments in Battery Thermal Management Systems for Electric Vehicles: A Technical Review." *Journal of Energy Storage* 35 (January): 102255. https://doi.org/10.1016/j.est.2021.102255.
- [34] Vahedi, Hani, Mohammad Sharifzadeh, and Kamal Al-Haddad. 2018. "Modified Seven-Level Pack U-Cell Inverter for Photovoltaic Applications." *IEEE Journal of Emerging and Selected Topics in Power Electronics* 6 (3): 1508–16. https://doi.org/10.1109/JESTPE.2018.2821663.
- [35] Vijeh, Mahdi, Mohammad Rezanejad, Emad Samadaei, and Kent Bertilsson. 2019. "A General Review of Multilevel Inverters Based on Main Submodules: Structural Point of View." *IEEE Transactions on Power Electronics* 34 (10): 9479–9502. https://doi.org/10.1109/TPEL.2018.2890649.